

Insight into the Mechanisms Driving the Self-Assembly of Functional Interfaces: Moving from Lipids to Charged Amphiphilic Oligomers

Azhad U. Chowdhury[‡], Graham J. Taylor[¶], Vera Bocharova[‡], Robert L. Sacci[‡], Yingdong Luo[§], Ying-Zhong Ma[‡], Stephen A. Sarles[†], Kunlun Hong[§], C. Patrick Collier^{*, §} Benjamin Doughty^{*, ‡}

Notice: This manuscript has been authored by UT-Battelle, LLC, under Contract No. DE-AC0500OR22725 with the U.S. Department of Energy. The United States Government retains and the publisher, by accepting the article for publication, acknowledges that the United States Government retains a non-exclusive, paid-up, irrevocable, world-wide license to publish or reproduce the published form of this manuscript, or allow others to do so, for the United States Government purposes.

Insight into the Mechanisms Driving the Self-Assembly of Functional Interfaces: Moving from Lipids to Charged Amphiphilic Oligomers

Azhad U. Chowdhury[‡], Graham J. Taylor[¶], Vera Bocharova[‡], Robert L. Sacchi[‡], Yingdong Luo[§], Ying-Zhong Ma[‡], Stephen A. Sarles[†], Kunlun Hong[§], C. Patrick Collier^{*,§}, Benjamin Doughty^{*,‡}

[‡]Chemical Sciences Division and [§]Center for Nanophase Materials Sciences, Oak Ridge National Laboratory, Oak Ridge, Tennessee 37831, United States

[¶]Bredesen Center for Interdisciplinary Research and [†]Department of Mechanical, Aerospace, and Biomedical Engineering, The University of Tennessee, Knoxville, Tennessee 37996, United States

KEYWORDS. *Nonlinear optics, ionic polymer stabilized interface, droplet interface bilayer*

ABSTRACT: Polymer-stabilized liquid-liquid interfaces are an important and growing class of bioinspired materials that combine the structural and functional capabilities of advanced synthetic materials with naturally evolved biophysical systems. These platforms have the potential to serve as selective membranes for chemical separations, molecular sequencers, and to even mimic neuromorphic computing elements. Despite the diversity in function, basic insight into the assembly of well-defined amphiphilic polymers to form functional structures remains elusive, which hinders the continued development of these technologies. In this work we provide new mechanistic insight into the assembly of an amphiphilic polymer-stabilized oil/aqueous interface, in which the headgroups consist of positively charged methylimidazolium ionic liquids, and the tails are short, monodisperse oligodimethylsiloxanes covalently attached to the headgroups. We demonstrate using vibrational sum frequency generation spectroscopy and pendant drop tensiometry that the composition of the bulk aqueous phase, particularly the ionic strength, dictates the kinetics and structures of the amphiphiles in the organic phase as they decorate the interface. These results show that H-bonding and electrostatic interactions taking place in the aqueous phase bias the grafted oligomer conformations that are adopted in the neighboring oil phase. The kinetics of self-assembly were ionic strength dependent and found to be surprisingly slow, being composed of distinct regimes where molecules adsorb and reorient on relatively fast time scales, but where conformational sampling and frustrated packing takes place over longer timescales. These results set the stage for understanding related chemical phenomena of bioinspired materials in diverse technological and fundamental scientific fields and provide a solid physical foundation on which to design new functional interfaces.

INTRODUCTION

Lipid bilayers are central to many biological functions and play a key role in numerous fundamental processes including the transport of ions/small molecules and mediating self-assembly of proteins.¹ The large range of lipid bilayer functions is accomplished through the diversity of lipid species that can modulate the membranes' physical and chemical properties. Synthetic approaches can build on this molecular diversity through the inclusion of designer amphiphilic oligomers and block copolymers that mimic the functionality of natural materials. These designer molecules can contain key structural and chemical "knobs" that potentially allow for control over membrane properties. Such amphiphilic polymers can self-assemble into synthetic nanoscale membranes with variable behaviors reminiscent of lipid-based membranes but are considerably more stable and robust than their natural counterparts.² The ability to incorporate membrane proteins into these synthetic bilayers provides access to many signal processing modalities: ion channels and pumps can be used to sequence DNA,³ to charge biobatteries,⁴ and to emulate hearing.⁵ Recently, these platforms have demonstrated the potential for using ion-channel doped planar bilayers as synapse-inspired memristors capable of integration in neuromorphic computing applications.^{6,7} Broadly speaking, these types of chemical/material platforms have the potential to act as the functional elements in complex devices capable of a wide range of functions. Despite this potential, fundamental insight into the assembly of these well-defined amphiphilic species into emergent structures remains elusive and therefore limits the continued development of relevant technologies.

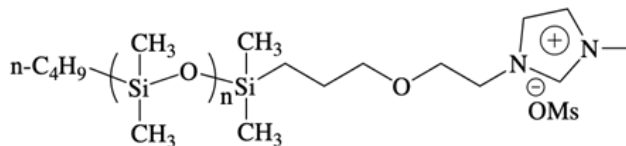


Figure 1: Structure of oligodimethylsiloxane imidazolium mesylate: ODMS-MIM⁽⁺⁾ OM⁽⁻⁾

Most polymer-based membranes are formed from block copolymers that self-assemble into well-characterized morphological phases.⁸ These supramolecular systems however are large and complex, which can result in long-range repulsive forces based on osmotic stress and other excluded volume interactions that hinder membrane formation and are difficult to characterize.⁹ In addition, membranes formed from block copolymers are compressible, and are typically much thicker than lipid bilayers, which complicates the search for design rules affecting their assembly. To circumvent these complications, ionic species can be introduced to membrane-forming polymers/oligomers to enhance their self-assembly via attractive electrostatic forces and increase their amphiphilicity at the oil/aqueous interface. In this work, we make use of the molecule sketched in Fig. 1, where we covalently linked a single ionic liquid (IL) unit (methylimidazolium cation, MIM⁽⁺⁾) to the chain end of a commercially available, discrete oligomer (oligodimethylsiloxane, ODMS, 1 kDa). The charged headgroups can self-assemble at the oil-aqueous interface to resemble a "grafted-to" polymer chain, but with graft points that are mobile along the liquid/liquid (L/L) phase boundary. The resulting system resembles model lipid

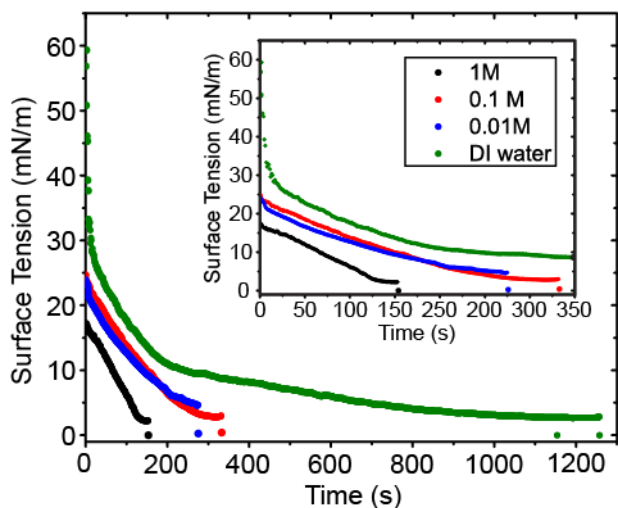


Figure 2: Monolayer surface tension measured during ionic oligomer self-assembly at an oil-aqueous interface at different NaCl concentrations in the aqueous phase, as indicated in the legend. The observed surface tension decreased over time as the amphiphilic oligomer self-assembled into a monolayer at the droplet interface. The inset is a zoom into shorter time dynamics for the same data.

monolayers and bilayers that are useful for studying biomembrane related processes. Despite this similarity, there are key fundamental questions regarding the assembly of even the most basic of amphiphilic-oligomer monolayers. For instance, how does the structuring of the ionic headgroups in the aqueous phase impact the organization of the nonpolar chains in the oil phase? The self-assembly of lipids at hydrophobic-hydrophilic interfaces is spontaneous due to directional, attractive interactions resulting from shape anisotropy and enthalpic forces (hydrogen bonds and π -stacking). In contrast, membrane formation for amphiphilic polymers often involves a more subtle interplay among various forces, including enthalpic and entropic forces.² Additionally, probing molecular assembly, structure and kinetics at these buried interfaces presents several technical challenges in isolating the interfacial species from the surrounding bulk phases.

Learning in detail the complex mechanisms governing the self-assembly of oligomer-based membranes in an attempt to mimic the structure and function of natural lipid bilayers can enable the discovery of design rules responsible for the emergence of complex and nonlinear dynamical behaviors in artificial and natural interfaces. Numerous examples linking assembly and function have been found for lipid-based membrane analogs, both with and without membrane-associated macromolecules like proteins. These include sharp concentration and voltage thresholds for ion channel insertion and conduction in lipid membranes due to first-order phase transitions associated with structural changes in membrane morphology,⁶⁻⁷ and changes in the state equations of lipid membranes that relate time-dependent structural changes of the bilayer with memristive and memcapacitive behaviors.⁶⁻⁷

To obtain key mechanistic insight, we track the kinetics of self-assembly and associated conformational/structural aspects of ODMS-MIM⁽⁺⁾ amphiphilic oligomers adsorbed to the oil/aqueous interface using vibrational sum frequency generation (vSFG) spectroscopy and pendant drop tensiometry (PDT). We found that the ionic strength of the bulk aqueous phase strongly

impacts the assembly kinetics and equilibrated confirmations of the amphiphiles in the oil phase. Our work shows that ODMS tail conformations are highly dependent on the ability of the charged MIM⁽⁺⁾ headgroups to pack at the interface as mediated by screening via electrolytes and changes in H-bonding in the aqueous phase. These results lay the groundwork for future studies of well-defined ionic oligomers and polymers at interfaces that approach the complexity of natural systems.

RESULTS AND DISCUSSION

To study the kinetics of self-assembly of ODMS-MIM⁽⁺⁾ amphiphilic ionic oligomers at an oil/aqueous interface we first performed PDT measurements (details in experimental section). Fig. 2 shows the interfacial tension as a function of time following the formation of an inverted droplet of hexadecane containing 2 mg/mL ODMS-MIM⁽⁺⁾ submerged in 10 mM MOPS (3-(N-morpholino) propanesulfonic acid) buffer at pH 7.06. The curves shown in Fig. 2 describe the kinetics of monolayer formation in the presence of various concentrations of NaCl in the aqueous phase (0, 0.01, 0.1, 1 M NaCl). Notably, at high electrolyte concentrations, e.g., 1 M NaCl, a rapid (~150 seconds) decrease of the surface tension to a value below ~5 mN/m was observed at which point the droplet detached from the needle. In contrast, at lower NaCl concentrations of 0.1 and 0.01 M, the surface tension decreased more slowly, but eventually reached a similar ~5 mN/m level after ~250 seconds. For droplets submerged in pure deionized water free of salts, the surface tension decreased even more slowly. The dynamic surface tension data obtained with pure water showed two distinct regimes during the monolayer formation process: the interfacial tension first decreased sharply and approximately linearly during the first ~200 seconds, after which the monolayer tension decreased more gradually to below 5 mN/m over the course of another ~30 minutes. The first and second regimes were consistent with prior descriptions of monolayer formation via fast initial diffusion-limited deposition of intact liposomes or reverse micelles, followed by a slower long-term adsorption/exchange limited regime that carried the monolayer to its equilibrium packing density.¹⁰ In all cases, the surface tension fell below 5 mN/m provided that enough time was allowed to pass (>10 minutes).

The strong correlation between salt concentration and the rate of monolayer self-assembly, specifically as inferred by the amount of time required for the tension to decrease to less than 5 mN/m, suggests that electrostatic screening of the adsorbed polymers serves to reduce electrostatic repulsion forces generated by the charged cationic methylimidazolium headgroups. This is evident from the data in Fig. 2, where the presence of NaCl apparently enables facile assembly of the ionic oligomers to the oil/aqueous droplet interface. The fact that each PDT measurement ultimately reaches the same minimum surface tension (<5 mN/m) implies that regardless of ionic strength in the aqueous phase, the same final coverage of ODMS-MIM⁽⁺⁾ is achieved at the L/L interface. This observation, however, appears to contradict an electrostatically mediated process as suggested by the rate of change in surface tension obtained from our PDT measurements. In other words, one might expect that unscreened charges at low ionic strengths would result in increased repulsion between the headgroups at the interface to yield overall lower surface coverages and packing efficiencies.

This apparent discrepancy indicates that there is more happening at the monolayer interface than can be deduced from PDT measurements alone.

To extract the missing information regarding the adsorption of ODMS-MIM⁽⁺⁾ ionic oligomers to the hexadecane-aqueous interface, we have employed vibrational sum frequency generation (vSFG) spectroscopy. vSFG is ideally suited to study buried L/L interfaces as it is a surface-specific spectroscopic technique, where species in centrosymmetric and isotropic bulk media do not generate appreciable signals due to symmetry.¹¹⁻²³ In contrast, at interfaces, where symmetry is broken, coherent vSFG signals can be readily detected, allowing for a glimpse into the ordering and local chemistry governing assembly. Details surrounding the vSFG measurements can be found in the experimental section and in recent reports.²⁴⁻²⁵ Complementary Raman and low temperature attenuated total reflection Fourier transform infrared spectra of the neat ODMS-MIM⁽⁺⁾ sample are also presented in Fig. S4 in the Supporting Information. The surface areas in the PDT and vSFG measurements are comparable within an order of magnitude.

Static vSFG spectra (i.e., samples allowed to equilibrate for >30 minutes) of ODMS-MIM⁽⁺⁾ at the hexadecane/aqueous interfaces in different polarization combinations and electrolyte concentrations are shown in Fig. 3. For both 1 M NaCl and 0.1 M NaCl (both in MOPS) aqueous phases, a pronounced band centered near 2909 cm⁻¹ was observed in the SSP polarization combination that we assign to the methyl symmetric stretch (-CH₃-*ss*) from the ODMS tail, in agreement with previous work,²⁶⁻²⁷ vSFG selection rules,¹⁴⁻¹⁵ and linear vibrational spectroscopies (Fig. S4). Similarly, the PPP and SPS spectra show peaks near 2964 cm⁻¹ that correspond to methyl asymmetric stretches (-CH₃-*as*) on the ODMS tail. This feature might also contain unresolved contributions from the CH₃-*ss* of the terminal imidazolium.²⁸⁻³⁰ Weak features appearing near 3014 cm⁻¹ correspond to the C(2)-H stretch on the imidazolium ring that is commonly associated with H-bonding interactions.²⁸⁻³⁰ The lack of strong signal from this peak, or other functional groups on the imidazolium group (e.g., methyl and H-C(4)-C(5)-H groups)²⁸⁻³¹ suggests that the imidazolium ring lays mostly parallel to the L/L interface with the C(2)-H bond pointing slightly into or out of the aqueous phase depending on the electrolyte concentration.

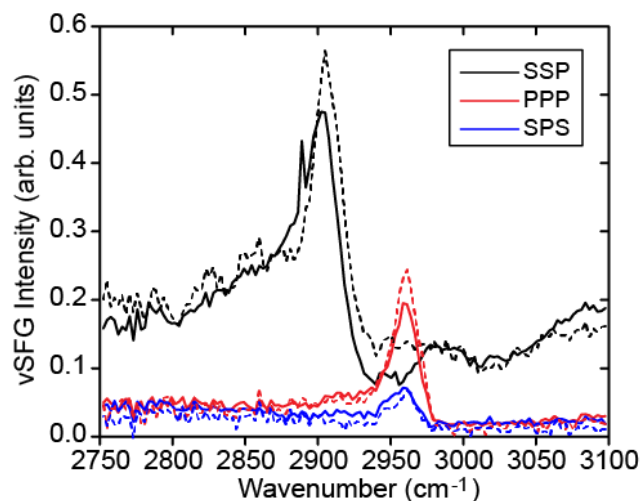


Figure 3: vSFG spectra in different polarization combinations from the ODMS-MIM⁽⁺⁾ oligomers at the hexadecane/0.1 M NaCl MOPS interface (solid lines) and hexadecane/1 M NaCl MOPS interface (dashed lines).

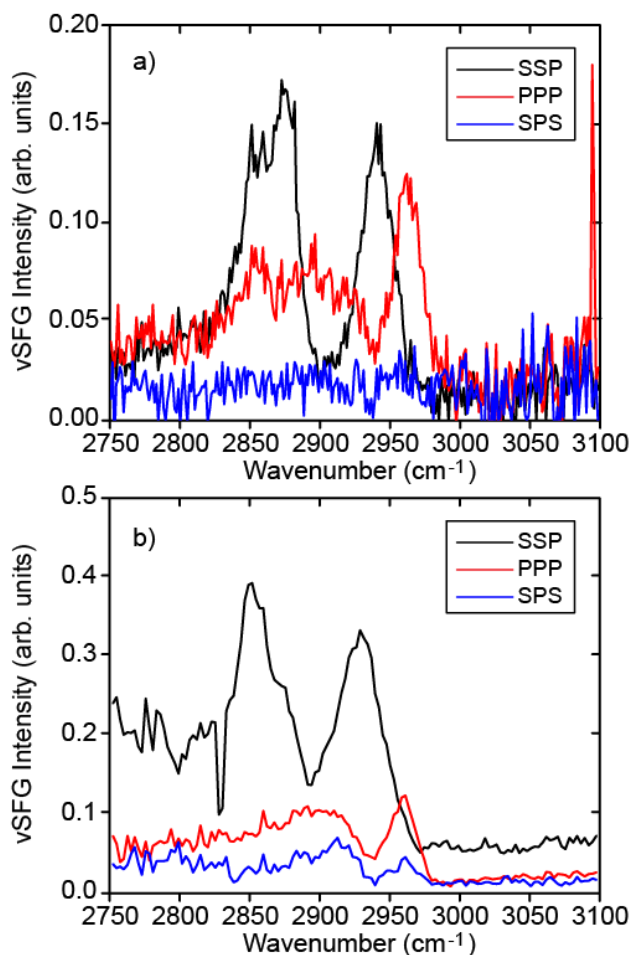


Figure 4: SFG spectra collected from: a) the hexadecane/aqueous interface and b) the ODMS-MIM⁽⁺⁾ in hexadecane/air interface with different polarization combinations as noted in the insets.

In fact, the amplitudes of this feature (data summarized in Tables S1 and S2) are of different sign for the two aqueous phases studied, which hints at subtly different orientations that the head groups can take in response to changing ionic strength in the bulk. Unfortunately, the weak signal for this band and its absence in other polarization combinations precludes a quantitative analysis of the molecular orientation. In the case of the SSP spectrum at 1 M NaCl, a weak feature at 2828 cm⁻¹ was also observed and is attributed to the mesylate counterion CH₃-*ss*.³² This indicates, as proposed elsewhere,³² that the counter anions can co-adsorb at the L/L interface at high bulk electrolyte concentrations. The very broad features near 2855 cm⁻¹ are likely due to unresolved contributions from methylene stretches (linker from imidazolium to ODMS), combination bands,³¹ and/or the terminal CH₃-*ss* on the ODMS-tail.^{28-30, 32} The broad signal extending from $\omega > 3100$ cm⁻¹ is due to the -OH stretch of water and indicates the presence of ordered water at the charged L/L interface.^{17, 33-35}

To confirm that the vSFG spectral features observed in Fig. 3 are truly from the ODMS-MIM⁽⁺⁾ ionic oligomer at the hexadecane/aqueous interface, we performed three separate control measurements: one probed the aqueous/air interface, another probed the aqueous/oil interface, and the third probed the polymer-in-oil/air interface. First, no signal was observed from the aqueous/air interface (Fig. S7), indicating that MOPS is not surface active at the present concentrations and is not responsible

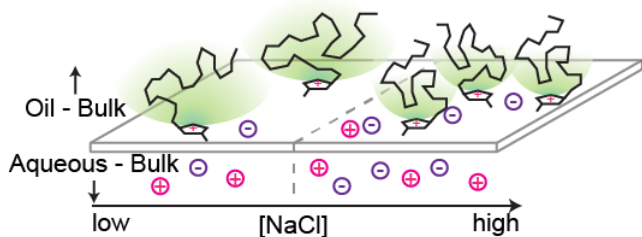


Figure 5: Cartoon illustrating the effect of electrolytes on surface ordering and packing on MIM-ODMS head groups and tails. The volume that the tails can sample is indicated by the green shaded region. Based on vSFG measurements, at high electrolyte concentrations (e.g., 1 M) the tails assume a more compact structure, which is mediated by charge screening of the head groups in the aqueous phase.

for the signals observed in Fig. 3. Next, the hexadecane/aqueous interface shown in Fig. 4a), shows three characteristic bands in the SSP spectrum at 2858, 2878, and 2942 cm^{-1} , and are assigned to $\text{CH}_2\text{-ss}$, $\text{CH}_3\text{-ss}$ and Fermi resonance of hexadecane, in agreement with previous vSFG studies.³⁶⁻³⁷ Similarly, the PPP spectra for the hexadecane/aqueous interface showed peaks at 2858, 2903, and 2965 cm^{-1} , corresponding to methylene symmetric stretches, methylene asymmetric stretches, and the asymmetric stretch of the terminal methyl groups of hexadecane.³⁶⁻³⁷ Notably, these features were not observed at the L/L interface in the presence of ODMS-MIM⁽⁺⁾ (Fig. 3). This means that the amphiphilic polymer displaced the hexadecane at the oil-water interface, as expected based on interfacial tension measurements. Finally, we performed measurements of the ODMS-MIM⁽⁺⁾ oligomer at the oil/air interface, as shown in Fig. 4b). The spectra obtained were like those at the neat oil-water interface, with similar peak positions and assignments for the various bands, but with different relative intensities. These differences are descriptive of different ordering of the hexadecane chains at the air versus aqueous interfaces, which have different polarities. The absence of characteristic ODMS-MIM⁽⁺⁾ bands in all control spectra indicates that the ODMS-MIM⁽⁺⁾ oligomer is the dominant surface-active species at the buried L/L interface and that we are indeed probing the ionic oligomer species located there.

Turning attention back to the data in Fig. 3, the relative peak intensities, areas, and widths, particularly for the ODMS-MIM⁽⁺⁾ $\text{CH}_3\text{-ss}$ band at 2909 cm^{-1} , vary depending on the ionic strength of the aqueous phase. The relative areas, amplitudes, and widths all report on different aspects of population, ordering, and local chemical heterogeneity, as will be discussed further below. First, the peak area for the $\text{CH}_3\text{-ss}$ from the 1 M NaCl aqueous phase sample is *smaller* than that of the 0.1 M NaCl sample (data in Table S1 and S2). At first glance, this might suggest that the population is lower at higher ionic strength; however, when one considers the intrinsic symmetry of the ODMS backbone (alternating methyl groups with high degree of rotational freedom about the bond axes), it becomes apparent that a smaller peak area describes both population *and* tail conformation. Namely, at the relatively low grafting densities used here, regardless of electrolyte concentration, the ODMS tails assume a coiled conformation in the so-called ‘mushroom’ regime³⁸⁻³⁹ (sketched in Fig. 5 - green shaded region). At the higher adsorption densities anticipated at 1 M NaCl, based on PDT measurements and electrostatic arguments, the footprint of the ODMS tails must necessarily be

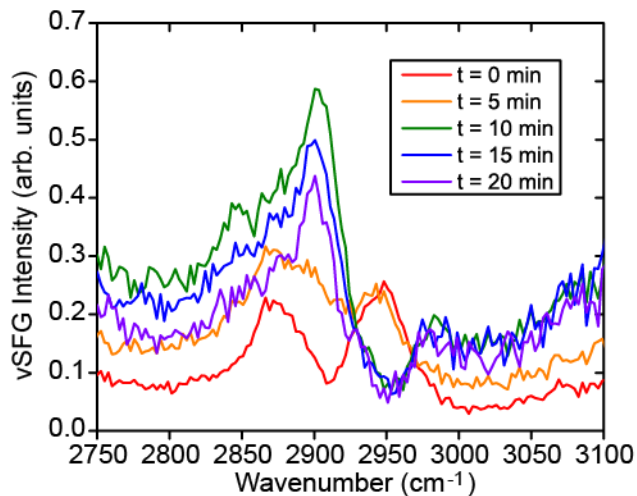


Figure 6: Time-resolved vSFG spectra acquired in the SSP polarization combination where the observed changes in band positions and relative amplitudes reflect displacement of oil from the oil/aqueous interface and the adsorption/ordering of the polymer.

smaller to accommodate an increase in the number of ionic oligomers at the L/L interface. This has the effect of either straightening out the tails or more tightly coiling them into smaller ‘mushrooms’ where, in either case, destructive interference of vSFG signals from oppositely orientated methyl groups will lower signal amplitudes despite the increase in overall number density. In contrast, at lower coverages and lower ionic strengths in the aqueous phase, larger peak areas are observed, consistent with the tails assuming more spread-out conformations with the methyl groups pointing into the oil phase (i.e., the ODMS backbone lays more parallel to the L/L interface with the methyl groups pointing into the oil phase to minimize interactions with the aqueous phase).²⁷ The same picture is also qualitatively reflected in the associated amplitudes for the $\text{CH}_3\text{-ss}$ mode.²⁶

This physical picture is further supported by considering the extracted spectral linewidths for the $\text{CH}_3\text{-ss}$ in the SSP spectra, which show overall narrower linewidths from the 1 M NaCl samples compared to the 0.1 M NaCl sample. Specifically, a linewidth of $\Gamma_{\text{CH}_3\text{-ss}} = 11.6 \pm 0.4 \text{ cm}^{-1}$ was recovered from the 1 M NaCl aqueous phase, whereas $\Gamma_{\text{CH}_3\text{-ss}} = 15.1 \pm 0.4 \text{ cm}^{-1}$ was observed for the 0.1 M NaCl solution. This observation indicates that the breadth of local chemical environments sampled by the tails is larger in the less confined ODMS-MIM⁽⁺⁾ adsorbed at the hexadecane/0.1 M NaCl aqueous interface. Similarly, the more tightly coiled/smaller footprint ODMS-MIM⁽⁺⁾ at the 1 M NaCl aqueous interface is less broadened likely due to better packing and buried methyl groups that do not interact with neighboring phases/molecules. This combined with the aforementioned subtle variations in the weak imidazolium vSFG signal indicates that the electrolytes play a key role in screening the charged head groups from one another at the oil/water interface. This screening allows for tighter assembly of head groups and a correspondingly smaller spatial volume near the surface that can be sampled by the ODMS tails.^{11, 40 41-42}

Time-Dependent Monolayer Formation probed via vSFG

To further validate the physical picture sketched in Fig.5 and discussed above, we performed time-resolved vSFG measure-

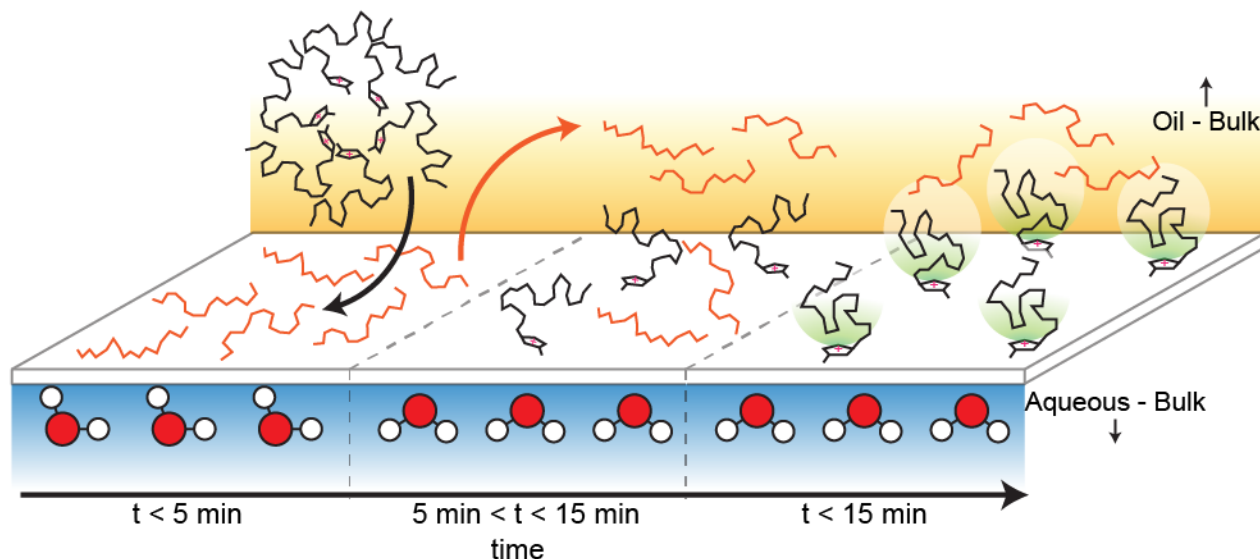


Figure 7: Illustration of adsorption and ordering kinetics as explained by vSFG and PDT measurements. At early times ($t < 5$ mins) the interface is predominantly composed of water and hexadecane with micelles of the ODMS-MIM⁽⁺⁾ ionic oligomer dissolved in the oil phase. As time progresses ($5 \text{ min} < t < 15 \text{ min}$), the micelles adsorb and break apart near the surface (black arrow) and begin populating the surface, displacing hexadecane (orange arrow). At long times, the surface coverage continues to increase, which is dictated by the ability to accommodate additional MIM-PDMS molecules at the interface.

ments to track in real-time the formation of the oligomer monolayer at the hexadecane/aqueous interface. This approach provides new insight into the dynamic ordering and molecular interactions taking place at the interface that cannot be provided by time-dependent changes in the measured interfacial tension. The results from kinetic vSFG measurements are shown in Fig. 6 and a corresponding physical model describing the kinetics is supplied in Fig. 7. On addition of the oligomer-in-oil solution to the 0.1 M NaCl aqueous phase, we observed a spectrum (at $t = 0$ mins) that matches the control oil/aqueous interface spectrum shown in Fig. 4a) which is dominated by signal from the hexadecane. As the ODMS-MIM⁽⁺⁾ self-assembles at the L/L interface, we observe that bands corresponding to hexadecane decrease in intensity, while a pronounced band at 2909 cm^{-1} , corresponding to the ODMS backbone, grows and eventually reaches a steady state at around 20 minutes that matches the static vSFG measurements presented in Fig. 3. Notably, the intensity of the ODMS $\text{CH}_3\text{-ss}$ is largest at moderate times (10-15 mins) *before* the equilibrated monolayer is formed. This is supportive of the idea that the ODMS tails initially organize along the surface plane with methyl groups pointing into the oil phase and the MIM⁽⁺⁾ interacting with the aqueous phase.²⁷ At longer times, more oligomers adsorb and force the extended ODMS tails into more compact conformations, thus decreasing the associated vSFG signal due to destructive interference. The timescale for interfacial adsorption and organization is in excellent agreement with the interfacial tension measurements, thus explaining the molecular origin of the changes observed. The vSFG kinetics show that even after initial adsorption, molecular events and additional packing of oligomers takes place on longer timescales to ultimately reach equilibrium. The apparent rate of adsorption is electrolyte dependent, but the PDT measurements only probe the population of ODMS-MIM⁽⁺⁾ at the interface up until it detaches from the needle at a surface tension of $\sim 5 \text{ mN/m}$. This means that the populations at equilibrium, as probed by vSFG, vary as a function of electrolyte concentration,

supporting a charge screening mechanism mediating adsorption. This suggests that in some cases, particularly when the sample interface can detach from the supporting needle, PDT measurements might not ever capture the final equilibrated interface. Additionally, we observe that on the higher frequency side of the time-resolved vSFG spectra (Fig. 6), the -OH vibrations of water at the interface increased as a function of time and on a faster timescale than the tail organization. The observation of ordered water is expected at charged interfaces due to the ionic imidazolium head groups polarizing water molecules near the interface.^{33, 43-44} Furthermore, at hydrophobic interfaces ($t < 5$ mins), water orients such that one -OH bond points into the oil phase (i.e., a ‘free-OH’), whereas on ODMS-MIM⁽⁺⁾ adsorption, the water must reorient to accommodate the positively charged imidazolium group such that the -OH groups are pointed into the aqueous phase,⁴⁵ as sketched in Fig. 7. Kinetic experiments attempted at 1 M NaCl conditions were found to evolve too quickly to resolve in time with vSFG, which is consistent with the physical picture described here and the PDT measurements presented above.

CONCLUSIONS

We have tracked in real time the self-assembly of a biomimetic ionic oligomer at the hexadecane/aqueous interface. Mechanistically, the results suggest that the ionic oligomers adsorb to the L/L interface and subsequently form a monolayer that reduces the interfacial tension and reorients water molecules and the associated H-bonding network at the interface. The ODMS-MIM⁽⁺⁾ molecules initially orient such that the charged imidazolium headgroup lays parallel to the L/L interface. Similarly, the ODMS tails initially lay parallel to the interface such that the associated methyl groups are pointed into the oil phase. As the system reaches the equilibrium configuration and maximum packing density at the surface, the tails eventually contort to accommodate neighboring oligomers to form an interfacial layer

in the so-called ‘mushroom’ regime.³⁸⁻³⁹ Importantly, the present results show that tail conformations in the oil phase are ultimately directed by electrostatic screening of charges in the aqueous phase, which is somewhat surprising since the electrolytes never directly interact with moieties in the oil phase. This electrostatic driven ordering in the oil phase is accomplished by altering the interaction of the charged head groups with each other and the overall H-bonding network of water at the interface. As such, one can change the overall packing conformation by tuning the electrostatics and H-bonding network using the aqueous phase composition. This acts as a potential ‘knob’ to tune self-assembly and function in bilayer devices and provides new insight into the design rules for these and related soft matter interfaces that can be leveraged in future work in this and related fields. We anticipate that this mechanistic insight into the assembly of these well-defined ionic oligomers will set the stage for future applications in biomimetic and neuromorphic applications. Results from this work may be directly applicable to advanced functional materials, brain complexity, and energy-efficient neuromorphic computing, as well as practical technological advances in sensors, separations, and detection technologies.

EXPERIMENTAL SECTION

ODMS-MIM⁽⁺⁾ Synthesis

Detailed procedures for the synthesis of the ODMS-MIM⁽⁺⁾ OMs⁽⁻⁾ ionic oligomers can be found in the supporting information along with NMR characterization.

PDT Measurements

Dynamic surface tension measurements were made to monitor polymer self-assembly at oil-water interfaces using a RameHart Pendant Drop Tensiometer. The polymer was dissolved in hexadecane at a concentration of 2 mg/mL, yielding an optically transparent bulk oil phase. Measurements were made as described previously^{10, 46} using 1-2 μ L inverted ODMS-MIM⁽⁺⁾ in oil droplets generated at the tip of a stainless steel needle submerged in a cuvette containing 3-4 mL of water or buffer. The needle was pre-loaded with 20 μ L of oligomer in hexadecane solution before being submerged in the cuvette containing water or buffer. The needle was bent into a j-shape in house and thoroughly cleaned with water and acetone before and after measurements.

ATR-FTIR Measurements

Attenuated Total Reflection Fourier Transform Infrared spectra (ATR-FTIR) were recorded on an Agilent Cary 680 spectrometer, using a diamond prism ATR accessory (GoldenGate, Specac). The ODMS-MIM⁽⁺⁾ OMs⁽⁻⁾ sample was dropped on the diamond crystal and sealed using a Cu cup and graphite gasket. Liquid nitrogen was poured into the Cu cup until bubbling stopped and the thermocouple in the graphite gasket held at -177 °C for 20 min. The mirror speed was 5 kHz, resolution was 2 cm^{-1} , and integrated over 254 spectra.

Raman Measurements

Raman spectra were obtained using a XploRA spectrometer (Horiba) coupled with an Olympus microscope equipped with a 10x (0.25 NA) objective. The ODMS-MIM⁽⁺⁾ sample was drop cast onto microscope cover glass for measurements. All spectra were obtained using a laser centered at 638 nm. The Raman scattered light was dispersed using an 1800 line/mm grating and filtered using a 100 μ m pinhole before detection.

vSFG Measurements

For static vSFG measurements, NaCl in MOPS buffer solutions were placed in a cleaned Teflon dish to which a hexadecane/polymer layer was deposited (sketched in supporting information, Fig. S1a) The thickness of this layer, based on the volume of oil added and the surface area of the Teflon dish, was <10 μ m thick, allowing for IR light to pass through without substantial attenuation.⁴⁷ The samples were allowed to equilibrate for ~30 minutes before static experiments began. For kinetic SFG measurements, experiments started immediately after addition of the polymer in oil solution; these spectra were acquired using 300 s exposure times, which allowed for modest spectral resolution while providing enough temporal resolution to capture the assembly and organization at the interface.

The output of a regenerative amplifier (Ti:Sapphire, Spectra Physics Spitfire Pro) producing ~6 W average power at 1 kHz with ~40 fs pulses centered near 800 nm was split into two optical paths: one path lead to a TOPAS-Prime Plus optical parametric amplifier with difference frequency mixer to produce mid-infrared (IR) light centered near 3000 cm^{-1} . A portion of the second path in the near infrared (NIR) was temporally stretched using a 4f-pulse shaper equipped with a 2-dimensional liquid crystal on silicon spatial light modulator to generate time-symmetric narrowband up-conversion pulses.²⁴⁻²⁵ The polarization of the IR light was purified using a wire-grid polarizer and subsequently rotated with a zero order half-waveplate. Similarly, the NIR light polarization was purified using a Glan-Taylor polarizer and rotated using a zero-order half-waveplate. The IR and NIR beams were combined in a colinear geometry before being focused on the sample at a ~60° angle with respect to the surface normal – after passing through the air-oil interface the refracted beams are incident on the L/L interface at an angle of ~37° (see Fig. S1a and S1b). The radiated vSFG signal was collected in a reflection geometry, polarization resolved with an achromatic half waveplate/Glan-Taylor polarizer combination and filtered with a 750 nm shortpass filter before being focused into the entrance slit of a spectrograph equipped with a CCD camera. Three polarization combinations were collected for each sample, where the letters in the abbreviation describes the polarization of light measured/used in experiments in decreasing energy (i.e., SSP = S-SFG, S-NIR, P-IR). vSFG spectra were background subtracted using co-specified regions of interest and scaled by the IR spectrum obtained from a gold reference sample in the PPP combination.⁴⁸⁻⁵⁰ The radiated vSFG intensity is proportional to the square of second-order nonlinear susceptibility of the sample, $\chi_{\text{eff}}^{(2)}$, and the driving laser fields, (E_{IR} and E_{NIR}):^{15, 33, 51-53}

$$I_{\text{SFG}} \propto |\chi_{\text{eff}}^{(2)} E_{\text{IR}} E_{\text{NIR}}|^2 \quad (1)$$

where the effective second-order nonlinear susceptibility, is the sum of resonant, $\chi_{\text{res}}^{(2)}$, and non-resonant $\chi_{\text{NR}}^{(2)}$ contributions:

$$\chi_{\text{eff}}^{(2)} = \chi_{\text{NR}}^{(2)} e^{i\phi} + \chi_{\text{res}}^{(2)} = \chi_{\text{NR}}^{(2)} e^{i\phi} + \sum_q \frac{A_q}{\omega_{\text{IR}} - \omega_q + i\Gamma_q} \quad (2)$$

where ω_{IR} are frequency components in the incident broadband IR pulse, A_q is related to the amplitude, which describes the interfacial population and associated molecular orientation, ω_q is the resonance transition frequency, Γ_q describes the linewidth for the q^{th} -mode, and ϕ is the phase angle. Notably, the nonresonant background can contain contributions from the static electric field setup at the interface by the charged headgroups^{33, 43-44, 54} via the product of the third order susceptibility of water and the surface potential, which is mixed into the resonant response via ϕ . Given that one cannot uniquely fit two nonresonant contributions of the same functional form (i.e., $\chi_{\text{NR}}^{(2)}$, + $\chi_{\text{water}}^{(3)}$, each with their own phases) we fit the data using a single nonresonant response and phase. Band positions, amplitudes, and bandwidths were extracted from the data by fitting it to Equations 1 and 2; the results of the curve fitting are provided in Table S1-5 in the Supporting information. Individual data with associated error bars and fits are also included in the supporting information (Figs. S5-S9).

ASSOCIATED CONTENT

AUTHOR INFORMATION

Corresponding Author

*doughtybl@ornl.gov

*collierpc@ornl.gov

ORCID

Azhad U. Chowdhury - 0000-0002-6735-815X

Graham J. Taylor - 0000-0001-8833-7705

Vera Bocharova - 0000-0003-4270-3866

Robert L. Sacci - 0000-0002-0073-5221

Yingdong Luo - 0000-0002-1945-0680

Ying-Zhong Ma - 0000-0002-8154-1006

Stephen A. Sarles - 0000-0002-6694-6451

Kunlun Hong - 0000-0002-2852-5111

C. Patrick Collier - 0000-0002-8198-793X

Benjamin Doughty - 0000-0001-6429-9329

Present Addresses

Author Contributions

A.U.C., Y.-Z. M. and B.D. carried out vSFG measurements and associated analysis. G.J.T. S.A.S. and C.P.C. carried out PDT measurements and analysis. V.B. performed Raman measurements. R.L.S. performed FTIR measurements. Y.L. and K.H. prepared the ODMS-MIM⁽⁺⁾ sample. The manuscript was written through contributions of all authors. All authors have given approval to the final version of the manuscript.

Funding Sources

A.U.C., Y.-Z. M., and B.D. were sponsored by the Laboratory Directed Research and Development Program of Oak Ridge National Laboratory, managed by UT-Battelle, LLC, for the U.S. Department of Energy. A portion of this research was conducted at the Center for Nanophase Materials Sciences, which is a DOE Office of Science User Facility. V.B. and R.L.S. were supported by the U.S. Department of Energy, Office of Science, Basic Energy Sciences, Materials Sciences and Engineering Division. S.A.S. acknowledges the National Science Foundation Grant NSF ECCS-1631472

ACKNOWLEDGMENT

B.D. would like to acknowledge fruitful conversations and feedback on the manuscript provided by Tessa R. Calhoun.

ABBREVIATIONS

vSFG – vibrational sum frequency generation, IR – mid-infrared, NIR – near infrared, ODMS-MIM⁽⁺⁾ – oligodimethylsiloxane–methylimidazolium, OMs⁰ – mesylate anion

REFERENCES

1. Yang, N. J.; Hinner, M. J., Getting Across the Cell Membrane: An Overview for Small Molecules, Peptides, and Proteins. In *Site-Specific Protein Labeling: Methods and Protocols*, Gautier, A.; Hinner, M. J., Eds. Springer New York: New York, NY, 2015; pp 29-53.
2. Nardin, C.; Winterhalter, M.; Meier, W., Giant Free-Standing ABA Triblock Copolymer Membranes. *Langmuir* **2000**, *16* (20), 7708-7712.
3. Howorka, S.; Cheley, S.; Bayley, H., Sequence-specific detection of individual DNA strands using engineered nanopores. *Nature Biotechnology* **2001**, *19* (7), 636-639.
4. Holden, M. A.; Needham, D.; Bayley, H., Functional Bionetworks from Nanoliter Water Droplets. *Journal of the American Chemical Society* **2007**, *129* (27), 8650-8655.
5. Tamaddoni, N.; Freeman, E. C.; Sarles, S. A., Sensitivity and directionality of lipid bilayer mechanotransduction studied using a revised, highly durable membrane-based hair cell sensor. *Smart Materials and Structures* **2015**, *24* (6), 065014.
6. Najem, J. S.; Taylor, G. J.; Weiss, R. J.; Hasan, M. S.; Rose, G.; Schuman, C. D.; Belianinov, A.; Collier, C. P.; Sarles, S. A., Memristive Ion Channel-Doped Biomembranes as Synaptic Mimics. *ACS Nano* **2018**, *12* (5), 4702-4711.
7. Najem, J. S.; Hasan, M. S.; Williams, R. S.; Weiss, R. J.; Rose, G. S.; Taylor, G. J.; Sarles, S. A.; Collier, C. P., Dynamical nonlinear memory capacitance in biomimetic membranes. *Nature Communications* **2019**, *10* (1), 3239.
8. Tamaddoni, N.; Taylor, G.; Hepburn, T.; Michael Kilbey, S.; Sarles, S. A., Reversible, voltage-activated formation of biomimetic membranes between triblock copolymer-coated aqueous droplets in good solvents. *Soft Matter* **2016**, *12* (23), 5096-5109.
9. Zha, R. H.; de Waal, B. F. M.; Lutz, M.; Teunissen, A. J. P.; Meijer, E. W., End Groups of Functionalized Siloxane Oligomers Direct Block-Copolymeric or Liquid-Crystalline Self-Assembly Behavior. *Journal of the American Chemical Society* **2016**, *138* (17), 5693-5698.
10. Venkatesan, G. A.; Lee, J.; Farimani, A. B.; Heiranian, M.; Collier, C. P.; Aluru, N. R.; Sarles, S. A., Adsorption Kinetics Dictate Monolayer Self-Assembly for Both Lipid-In and Lipid-Out Approaches to Droplet Interface Bilayer Formation. *Langmuir* **2015**, *31* (47), 12883-12893.
11. Doughty, B.; Yin, P.; Ma, Y.-Z., Adsorption, Ordering, and Local Environments of Surfactant-Encapsulated Polyoxometalate Ions Probed at the Air-Water Interface. *Langmuir* **2016**, *32* (32), 8116-8122.
12. Voylov, D. N.; Holt, A. P.; Doughty, B.; Bocharova, V.; Meyer III, H. M.; Cheng, S.; Martin, H.; Dadmun, M.; Kisliuk, A.; Sokolov, A. P., Unraveling the molecular weight dependence of interfacial interactions in poly (2-vinylpyridine)/silica nanocomposites. *ACS Macro Letters* **2017**, *6* (2), 68-72.
13. Watson, B. R.; Ma, Y.-Z.; Cahill, J. F.; Doughty, B.; Calhoun, T. R., Probing ligand removal and ordering at quantum dot surfaces using vibrational sum frequency generation spectroscopy. *Journal of Colloid and Interface Science* **2019**, *537*, 389-395.

14. Lu, R.; Gan, W.; Wu, B.-h.; Zhang, Z.; Guo, Y.; Wang, H.-f., C-H Stretching Vibrations of Methyl, Methylene and Methine Groups at the Vapor/Alcohol (n = 1-8) Interfaces. *The Journal of Physical Chemistry B* **2005**, *109* (29), 14118-14129.
15. Wang *, H.-F.; Gan † ‡, W.; Lu † ‡ §, R.; Rao † ‡ ¶, Y.; Wu †, B.-H., Quantitative spectral and orientational analysis in surface sum frequency generation vibrational spectroscopy (SFG-VS). *International Reviews in Physical Chemistry* **2005**, *24* (2), 191-256.
16. Yan, E. C. Y.; Fu, L.; Wang, Z.; Liu, W., Biological Macromolecules at Interfaces Probed by Chiral Vibrational Sum Frequency Generation Spectroscopy. *Chemical Reviews* **2014**, *114* (17), 8471-8498.
17. Beaman, D. K.; Robertson, E. J.; Richmond, G. L., Ordered polyelectrolyte assembly at the oil-water interface. *Proceedings of the National Academy of Sciences* **2012**, *109* (9), 3226-3231.
18. Hankett, J. M.; Liu, Y.; Zhang, X.; Zhang, C.; Chen, Z., Molecular level studies of polymer behaviors at the water interface using sum frequency generation vibrational spectroscopy. *Journal of Polymer Science Part B: Polymer Physics* **2013**, *51* (5), 311-328.
19. Robertson, E. J.; Richmond, G. L., Molecular Insights in the Structure and Layered Assembly of Polyelectrolytes at the Oil/Water Interface. *The Journal of Physical Chemistry C* **2014**, *118* (49), 28331-28343.
20. Robertson, E. J.; Richmond, G. L., Chunks of Charge: Effects at Play in the Assembly of Macromolecules at Fluid Surfaces. *Langmuir* **2013**, *29* (35), 10980-10989.
21. Schabes, B. K.; Altman, R. M.; Richmond, G. L., Come Together: Molecular Details into the Synergistic Effects of Polymer-Surfactant Adsorption at the Oil/Water Interface. *The Journal of Physical Chemistry B* **2018**, *122* (36), 8582-8590.
22. Zhang, C., Sum Frequency Generation Vibrational Spectroscopy for Characterization of Buried Polymer Interfaces. *Appl. Spectrosc.* **2017**, *71* (8), 1717-1749.
23. Wanhala, A. K.; Doughty, B.; Bryantsev, V. S.; Wu, L.; Mahurin, S. M.; Jansone-Popova, S.; Cheshire, M. C.; Navrotsky, A.; Stack, A. G., Adsorption mechanism of alkyl hydroxamic acid onto bastnäsite: Fundamental steps toward rational collector design for rare earth elements. *Journal of Colloid and Interface Science* **2019**, *553*, 210-219.
24. Chowdhury, A. U.; Liu, F.; Watson, B. R.; Ashkar, R.; Katsaras, J.; Patrick Collier, C.; Lutterman, D. A.; Ma, Y.-Z.; Calhoun, T. R.; Doughty, B., Flexible approach to vibrational sum-frequency generation using shaped near-infrared light. *Opt. Lett.* **2018**, *43* (9), 2038-2041.
25. Chowdhury, A. U.; Watson, B. R.; Ma, Y.-Z.; Sacci, R. L.; Lutterman, D. A.; Calhoun, T. R.; Doughty, B., A new approach to vibrational sum frequency generation spectroscopy using near infrared pulse shaping. *Review of Scientific Instruments* **2019**, *90* (3), 033106.
26. Zhang, C.; Chen, Z., Probing Molecular Structures of Poly(dimethylsiloxane) at Buried Interfaces in Situ. *The Journal of Physical Chemistry C* **2013**, *117* (8), 3903-3914.
27. Kim, C.; Gurau, M. C.; Cremer, P. S.; Yu, H., Chain Conformation of Poly(dimethyl siloxane) at the Air/Water Interface by Sum Frequency Generation. *Langmuir* **2008**, *24* (18), 10155-10160.
28. Baldelli, S., Surface Structure at the Ionic Liquid-Electrified Metal Interface. *Accounts of Chemical Research* **2008**, *41* (3), 421-431.
29. Rivera-Rubero, S.; Baldelli, S., Surface Characterization of 1-Butyl-3-methylimidazolium Br⁻, I⁻, PF₆⁻, BF₄⁻, (CF₃SO₂)₂N⁻, SCN⁻, CH₃SO₃⁻, CH₃SO₄⁻, and (CN)₂N⁻ Ionic Liquids by Sum Frequency Generation. *The Journal of Physical Chemistry B* **2006**, *110* (10), 4756-4765.
30. Romero, C.; Baldelli, S., Sum Frequency Generation Study of the Room-Temperature Ionic Liquids/Quartz Interface. *The Journal of Physical Chemistry B* **2006**, *110* (12), 6213-6223.
31. Carter, D. A.; Pemberton, J. E., Raman spectroscopy and vibrational assignments of 1- and 2-methylimidazole. *Journal of Raman Spectroscopy* **1997**, *28* (12), 939-946.
32. Deng, G.-H.; Li, X.; Liu, S.; Zhang, Z.; Lu, Z.; Guo, Y., Successive Adsorption of Cations and Anions of Water-1-Butyl-3-methylimidazolium Methylsulfate Binary Mixtures at the Air-Liquid Interface Studied by Sum Frequency Generation Vibrational Spectroscopy and Surface Tension Measurements. *The Journal of Physical Chemistry C* **2016**, *120* (22), 12032-12041.
33. Ohno, P. E.; Wang, H.-f.; Geiger, F. M., Second-order spectral lineshapes from charged interfaces. *Nature Communications* **2017**, *8* (1), 1032.
34. Dutta, C.; Svirida, A.; Mammetkuliyeu, M.; Rukhadze, M.; Benderskii, A. V., Insight into Water Structure at the Surfactant Surfaces and in Microemulsion Confinement. *The Journal of Physical Chemistry B* **2017**, *121* (31), 7447-7454.
35. McFearin, C. L.; Richmond, G. L., The Role of Interfacial Molecular Structure in the Adsorption of Ions at the Liquid-Liquid Interface. *The Journal of Physical Chemistry C* **2009**, *113* (50), 21162-21168.
36. Chen, Y.; Jena, K. C.; Roke, S., From Hydrophobic to Hydrophilic: The Structure and Density of the Hexadecane Droplet/Alkanol/Water Interface. *The Journal of Physical Chemistry C* **2015**, *119* (31), 17725-17734.
37. Scheu, R.; Chen, Y.; de Aguiar, H. B.; Rankin, B. M.; Ben-Amotz, D.; Roke, S., Specific Ion Effects in Amphiphile Hydration and Interface Stabilization. *Journal of the American Chemical Society* **2014**, *136* (5), 2040-2047.
38. Egorov, S. A.; Hsu, H.-P.; Milchev, A.; Binder, K., Semiflexible polymer brushes and the brush-mushroom crossover. *Soft Matter* **2015**, *11* (13), 2604-2616.
39. Brittain, W. J.; Minko, S., A structural definition of polymer brushes. *Journal of Polymer Science Part A: Polymer Chemistry* **2007**, *45* (16), 3505-3512.
40. Weeraman, C.; Yatawara, A. K.; Bordenyuk, A. N.; Benderskii, A. V., Effect of Nanoscale Geometry on Molecular Conformation: Vibrational Sum-Frequency Generation of Alkanethiols on Gold Nanoparticles. *Journal of the American Chemical Society* **2006**, *128* (44), 14244-14245.
41. Barrett, A.; Petersen, P. B., Order of Dry and Wet Mixed-Length Self-Assembled Monolayers. *The Journal of Physical Chemistry C* **2015**, *119* (42), 23943-23950.
42. Algou, S. T.; Sengupta, S.; Bui, T. T.; Velarde, L., Tuning the Surface Ordering of Self-Assembled Ionic Surfactants on Semiconducting Single-Walled Carbon Nanotubes: Concentration, Tube Diameter, and Counterions. *Langmuir* **2018**, *34* (31), 9279-9288.
43. Zhao, X.; Ong, S.; Wang, H.; Eisenthal, K. B., New method for determination of surface pKa using second harmonic generation. *Chemical Physics Letters* **1993**, *214* (2), 203-207.
44. Zhao, X.; Subrahmanyam, S.; Eisenthal, K. B., Determination of pKa at the air/water interface by second harmonic generation. *Chemical Physics Letters* **1990**, *171* (5), 558-562.
45. Mondal, J. A.; Nihonyanagi, S.; Yamaguchi, S.; Tahara, T., Structure and Orientation of Water at Charged Lipid Monolayer/Water Interfaces Probed by Heterodyne-Detected Vibrational Sum Frequency Generation Spectroscopy. *Journal of the American Chemical Society* **2010**, *132* (31), 10656-10657.
46. Venkatesan, G. A.; Taylor, G. J.; Basham, C. M.; Brady, N. G.; Collier, C. P.; Sarles, S. A., Evaporation-induced monolayer compression improves droplet interface bilayer formation using unsaturated lipids. *Biomicrofluidics* **2018**, *12* (2), 024101.
47. Nicolau, B. G.; García-Rey, N.; Dryzhakov, B.; Dlott, D. D., Interfacial Processes of a Model Lithium Ion Battery Anode Observed, in Situ, with Vibrational Sum-Frequency Generation Spectroscopy. *The Journal of Physical Chemistry C* **2015**, *119* (19), 10227-10233.

48. Tan, S.; Gray, M. B.; Kidder, M. K.; Cheng, Y.; Daemen, L. L.; Lee, D.; Lee, H. N.; Ma, Y.-Z.; Doughty, B.; Lutterman, D. A., Insight into the Selectivity of Isopropanol Conversion at Strontium Titanate (100) Surfaces: A Combination Kinetic and Spectroscopic Study. *ACS Catalysis* **2017**, *7* (12), 8118-8129.
49. Doughty, B.; Goverapet Srinivasan, S.; Bryantsev, V. S.; Lee, D.; Lee, H. N.; Ma, Y.-Z.; Lutterman, D. A., Absolute Molecular Orientation of Isopropanol at Ceria (100) Surfaces: Insight into Catalytic Selectivity from the Interfacial Structure. *The Journal of Physical Chemistry C* **2017**, *121* (26), 14137-14146.
50. Hu, X.; Wei, F.; Wang, H.; Wang, H., α -Quartz Crystal as Absolute Intensity and Phase Standard in Sum-Frequency Generation Vibrational Spectroscopy. *The Journal of Physical Chemistry C* **2019**.
51. Shen, Y. R., Phase-Sensitive Sum-Frequency Spectroscopy. *Annual Review of Physical Chemistry* **2013**, *64* (1), 129-150.
52. Chen, Z.; Shen, Y. R.; Somorjai, G. A., STUDIES OF POLYMER SURFACES BY SUM FREQUENCY GENERATION VIBRATIONAL SPECTROSCOPY. *Annual Review of Physical Chemistry* **2002**, *53* (1), 437-465.
53. Ye, S.; Tong, Y.; Ge, A.; Qiao, L.; Davies, P. B., Interfacial Structure of Soft Matter Probed by SFG Spectroscopy. *The Chemical Record* **2014**, *14* (5), 791-805.
54. Gonella, G.; Lütgebaucks, C.; de Beer, A. G. F.; Roke, S., Second Harmonic and Sum-Frequency Generation from Aqueous Interfaces Is Modulated by Interference. *The Journal of Physical Chemistry C* **2016**, *120* (17), 9165-9173.

